AFRL-RX-WP-TP-2010-4058

PROBABILISTIC FRETTING FATIGUE LIFE PREDICTION OF Ti-6Al-4V (PREPRINT)

Patrick J. Golden

Metals Branch
Metals, Ceramics & NDE Division

Harry R. Millwater and Xiaobin Yang

University of Texas at San Antonio

JANUARY 2010

AIR FORCE RESEARCH LABORATORY
MATERIALS AND MANUFACTURING DIRECTORATE
WRIGHT-PATTERSON AIR FORCE BASE, OH 45433-7750
AIR FORCE MATERIEL COMMAND
UNITED STATES AIR FORCE

REPORT DOCUMENTATION PAGE

Form Approved
OMB No. 0704-0188

1. REPORT DATE *(DD-MM-YY)*	2. REPORT TYPE	3. DATES COVERED *(From - To)*
January 2010	Journal Article Preprint	01 January 2010 – 31 January 2010

4. TITLE AND SUBTITLE
PROBABILISTIC FRETTING FATIGUE LIFE PREDICTION OF Ti-6Al-4V (PREPRINT)

5a. CONTRACT NUMBER
FA8650-04-C-5200

5b. GRANT NUMBER

5c. PROGRAM ELEMENT NUMBER
62102F

6. AUTHOR(S)
Patrick J. Golden (AFRL/RXLM)
Harry R. Millwater and Xiaobin Yang (University of Texas at San Antonio)

5d. PROJECT NUMBER
4347

5e. TASK NUMBER
RG

5f. WORK UNIT NUMBER
M02R3000

7. PERFORMING ORGANIZATION NAME(S) AND ADDRESS(ES)
Metals Branch (AFRL/RXLM)
Metals, Ceramics & NDE Division
Materials and Manufacturing Directorate
Wright-Patterson Air Force Base, OH 45433-7750
Air Force Materiel Command, United States Air Force

University of Texas at San Antonio
San Antonio, TX 78249

8. PERFORMING ORGANIZATION REPORT NUMBER

9. SPONSORING/MONITORING AGENCY NAME(S) AND ADDRESS(ES)
Air Force Research Laboratory
Materials and Manufacturing Directorate
Wright-Patterson Air Force Base, OH 45433-7750
Air Force Materiel Command
United States Air Force

10. SPONSORING/MONITORING AGENCY ACRONYM(S)
AFRL/RXLMN

11. SPONSORING/MONITORING AGENCY REPORT NUMBER(S)
AFRL-RX-WP-TP-2010-4058

12. DISTRIBUTION/AVAILABILITY STATEMENT
Approved for public release; distribution unlimited.

13. SUPPLEMENTARY NOTES
Journal article submitted to *International Journal of Fatigue*. PAO Case Number: 88ABW-2009-4305; Clearance Date: 07 Oct 2009. The U.S. Government is joint author of this work and has the right to use, modify, reproduce, release, perform, display, or disclose the work.

Part of AFRL Program: Life Prediction and Durability of Aerospace Materials.

14. ABSTRACT
A probabilistic analysis of the fatigue life of specimens subject to fretting fatigue was developed. A mechanics based fretting life analysis was applied that employed the local stress gradient at the edge of contact. The random variables in the analysis included the initial crack size, coefficient of friction, crack growth rate law, and the contact pad profile. The variation in pad profiles was determined through measurement of seventy-seven machined pads. Distributions for the other random variables were obtained using previously generated test data. A probabilistic fatigue analysis was applied using Monte Carlo sampling to determine the statistics (mean and standard deviation) of the fatigue life prediction and was compared to fretting fatigue test data. Several qualitative and quantitative sensitivity methods were applied to the results including the calculation of the probabilistic sensitivities (partial derivatives of the fatigue life statistics with respect to the input probability density function parameters) via linear regression and finite difference.

15. SUBJECT TERMS
probabilistic analysis, sensitivities, fretting fatigue, crack propagation

16. SECURITY CLASSIFICATION OF:			17. LIMITATION OF ABSTRACT:	18. NUMBER OF PAGES	19a. NAME OF RESPONSIBLE PERSON (Monitor)
a. REPORT	b. ABSTRACT	c. THIS PAGE			Reji John
Unclassified	Unclassified	Unclassified	SAR	40	19b. TELEPHONE NUMBER *(Include Area Code)* N/A

Standard Form 298 (Rev. 8-98)
Prescribed by ANSI Std. Z39-18

Probabilistic Fretting Fatigue Life Prediction of Ti-6Al-4V

Patrick J. Golden[1]
Materials and Manufacturing Directorate, Air Force Research Laboratory, Wright-Patterson AFB, OH 45433, USA

Harry R. Millwater and Xiaobin Yang
University of Texas at San Antonio, San Antonio, TX 78249, USA

Abstract

A probabilistic analysis of the fatigue life of specimens subject to fretting fatigue was developed. A mechanics based fretting life analysis was applied that employed the local stress gradient at the edge of contact. The random variables in the analysis included the initial crack size, coefficient of friction, crack growth rate law, and the contact pad profile. The variation in pad profiles was determined through measurement of seventy-seven machined pads. Distributions for the other random variables were obtained using previously generated test data. A probabilistic fatigue analysis was applied using Monte Carlo sampling to determine the statistics (mean and standard deviation) of the fatigue life prediction and was compared to fretting fatigue test data. Several qualitative and quantitative sensitivity methods were applied to the results including the calculation of the probabilistic sensitivities (partial derivatives of the fatigue life statistics with respect to the input probability density function parameters) via linear regression and finite difference.

[1] Materials Research Engineer, 2230 Tenth St, Ste 1, Wright-Patterson AFB, OH 45433-7817, USA, Phone: 937-255-5438, FAX: 937-656-4840, E-mail: patrick.golden@wpafb.af.mil

Keywords

Probabilistic Analysis, Sensitivities, Fretting Fatigue, Crack Propagation

1. Introduction

Fretting is a problem in many aerospace applications including the blade to disk attachment in turbine engines. Two fretting modes often contribute to damage in fretting: gross slip when the two surfaces slide resulting in wear, and partial slip when the two surfaces are nominally stuck together except for a small slip zone at the edge of contact. The surface damage and wear caused by fretting is a costly maintenance burden and when combined with the very high local contact stresses due to fretting, it can result in disk or blade cracking and the potential for catastrophic failure. Understanding of these damage mechanisms associated with fretting and accurate life prediction tools is critical to the sustainment of aerospace components.

Many approaches have been employed to aid in the life prediction of components with fretting. One approach is the use of material stress or strain-life curves with a "knockdown factor" determined through testing of specimens with fretting behavior similar to a component, or with actual or simulated components. This has the disadvantage, however, of being applicable to only a specific problem. Other approaches include development of critical lifing parameters that account for combinations of slip, applied stress, and/or strain [1,2]. These models are more general, but are typically calibrated to specimen data which may not fully account for the different geometry and stress gradients present in a component. Others have applied an approach that uses the local contact stress calculation combined with traditional multiaxial lifing tools, such as the Smith-Watson-Topper or equivalent stress parameters [3,4], and often combined with fracture mechanics fatigue crack growth [5-7]. This approach is well suited to fretting fatigue

problems that are dominated by partial-slip fretting since the surface damage and the high crack growth driving stresses are both localized at the edge of contact.

A probabilistic analysis is often applied to problems to help determine the effect of variability of the model input parameters on the model outputs. Prior work on statistical or probabilistic analysis in fretting includes modeling of the variability in the contact surface profile by Kumari and Farris [8]. Here, the measured profiles of the indentors in fretting fatigue tests were measured and statistically described and carried through the life prediction models to estimate the expected variability in stress and life. Other probabilistic fretting analyses include work on fretting fatigue of riveted lap joints [9] and on rolling contact [10]. In any probabilistic analysis it is crucial to understand which are the important random variables driving the results of the analysis. Importance is a combination of those that to which the results are the most sensitive and that are alterable with the least cost.

The objective of the current work was to develop and demonstrate a probabilistic fretting fatigue lifing approach for a dovetail fretting experimental configuration that included a broad range of input random variables, and to apply efficient sensitivity methods to determine the relative importance of the input variables. A previously demonstrated stress fracture mechanics based model was chosen for life prediction from small fretting crack to failure was adapted to this effort. Input probability density functions (PDF's) were developed using available laboratory data. Measures were applied to the analysis to determine qualitatively and quantitatively the random variable parameters that resulted in the highest results sensitivity.

2. Deterministic Analysis

A series of fretting experiments was previously conducted [11] to improve understanding of fretting behavior in Ti-6Al-4V and to assess life prediction models. The geometry of the

fretting samples was a dovetail shaped specimen that was designed to represent the attachment between a turbine engine blade and disk. The tests were conducted at room temperature, which is consistent with the operating conditions of a fan disk. The contact interface was bare Ti-6Al-4V on bare Ti-6Al-4V, but several coatings and residual stress surface treatments applied to the contact interface were also tested. The analysis in the current work was limited to the bare Ti-6Al-4V tests. A schematic of the fretting fatigue test rig modeled in this analysis is shown in Figure 1. The experimental setup consists of the dovetail specimen (one-half of the specimen is shown in the schematic), two fretting pads, and a steel fixture. Here, E_1 and ν_1 are the Young's modulus and Poissons Ratio of the specimen, respectively, and E_2 and ν_2 aret eh Young's Modulus and Poisson's ratio of the pad, respectively. Both the dovetail specimen and pads were machined from Ti-6Al-4V with a thickness of 7.62 mm, Young's modulus E = 116 GPa, and Poisson's ratio ν = 0.31. The fretting pads are held in the steel fixture at a 45° flank angle, and the dovetail specimen is pulled with a cyclic load, F, into the fretting pads. Both the dovetail specimen and pads were machined from Ti-6Al-4V with a thickness of 7.62 mm, modulus E = 116 GPa, and Poisson's ratio ν = 0.31. The nominal fretting pad geometry was a 3 mm flat with 3 mm blending radii. The normal, P, and shear, Q, contact forces were measured indirectly from strain gage instrumentation of the experiments. More details of the experimental setup and instrumentation can be found in Golden and Nicholas [11]. 10 tests were run at values of F_{max} ranging from 18 kN to 30 kN at a load ratio R = 0.1.

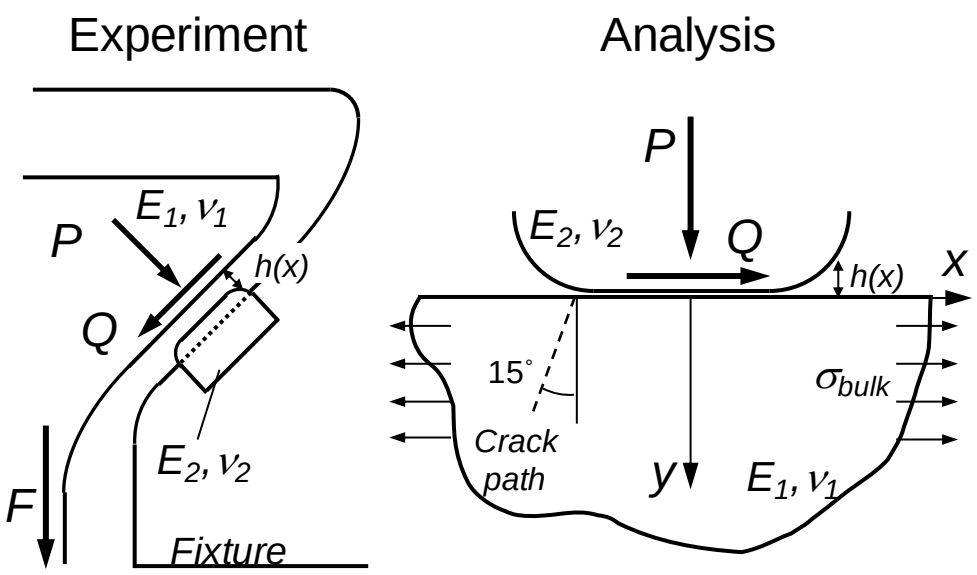

Figure 1: Schematic of the dovetail experiment and the analysis.

A fracture mechanics based fretting life prediction analysis for dovetail specimens was developed and demonstrated using these and other experimental test data and is described in Golden and Calcaterra [12]. The objective of this prior work was to demonstrate lifing methods that could be applied to more complex 3-D structures found in turbine engines, however, the current problem can be simplified to a 2-D problem. The analysis was broken into two parts: a finite element method (FEM) analysis and a 2-D numerical contact stress analysis. A finite element analysis is needed in this problem to determine two sets of quantities. The first quantity, described here, relates to the behavior of the contact force history. The second, which can be obtained from the same FEM model, is the bulk stress as shown in Figure 1 and is described below. The dovetail geometry was modeled using a nonlinear contact FEM model. This analysis yielded the contact force history for *P* and *Q* and an example is plotted in Figure 2. This example shows a single loading and unloading starting from zero load. As the load was applied, the contact was initially in sliding (gross slip) and the contact forces followed the dashed line defined by the equation

$$Q = \mu P \tag{1}$$

where μ is the coefficient of friction. Upon load reversal, the contact load path changes slope to the partial slip slope, α, which was positive in this case. In real components the slope, α, could range from a negative to a positive value including an infinite or vertical slope and is dependent on the component geometry and compliance. The contact forces will follow the slope α for both increasing and decreasing loads according to the equation

$$\Delta Q = \alpha \Delta P \tag{2}$$

until the dashed lines defining friction are reached according to Equation 1 for increasing load or the equation

$$Q = -\mu P \tag{3}$$

for decreasing load. Therefore, the two key inputs needed for prediction of the contact force history for a given applied load history were μ and α. The coefficient of friction, μ, is a property that can only be measured, however, α was predicted from the FEM analysis and confirmed by experimental measurement. Once these 2 parameters were known, the contact forces could be determined for a given applied force without additional FEM analysis through a procedure developed by Gean and Farris [13]. The procedure is outlined as follows and has also been used on a dovetail application in [14]. The remote applied force, *F*, and contact forces *P* and *Q* must satisfy the equation

$$F = P \sin\theta + Q \cos\theta \tag{4}$$

where θ is the dovetail flank angle. Additionally, the only valid values of *P* and *Q* were bounded by Equations 1 and X. If the applied force *F* is increasing, the *Q* versus i path will always move up with either a slope μ or α: μ if the current location is already on the line defined by Equation 1, and α if the current location is below that line. Likewise, if *F* is decreasing, the *Q*

versus P path will always move to the left with slope $-\mu$ if the current location is already on the line defined by Equation 3, or down with a slope α if the current location is above that line.

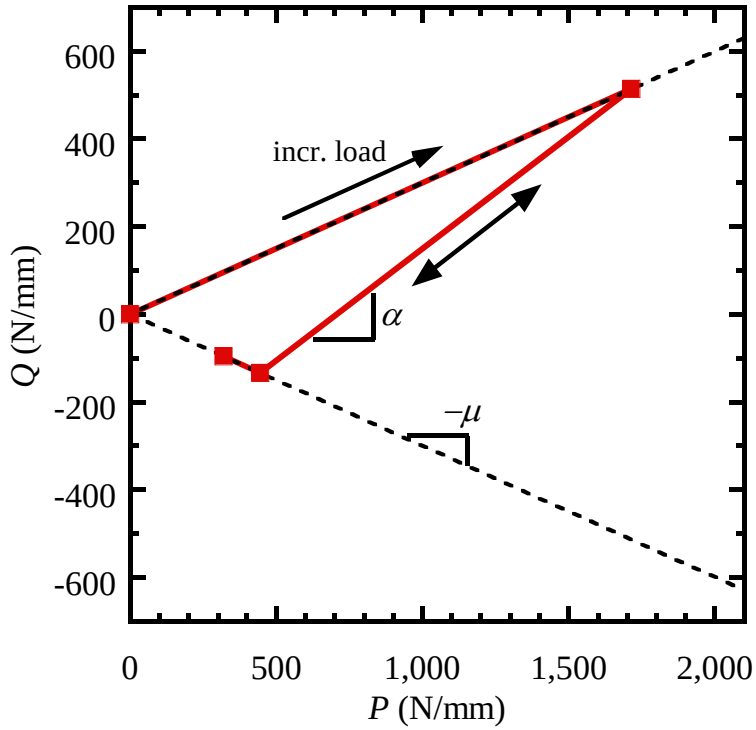

Figure 2: A typical plot of Q versus P showing the partial slip slope α and the boundaries defined by μ

Once the contact force history was known, the contact stresses were calculated using a 2-D numerical contact stress analysis. Figure 1 shows a schematic of the equivalent contact geometry, defined by the gap function, $h(x)$, used in this analysis. In the experiments described here, $h(x)$ was simply the profile of the fretting pads that are pressed into contact with the flat dovetail specimens. Rather than use the prescribed profile in the analysis, the as-machined profiles were measured using a contacting profilometer. The analytical tool, CAPRI (Contact Analysis for Profiles of Random Indenters) described in McVeigh et al. [15], was developed to solve the singular integral equation that defines this contact problem using any reasonable

function, $h(x)$, as measured from the profilometry. The output of CAPRI is the pressure, $p(x)$, and shear, $q(x)$, tractions due to the applied contact forces. An example of these tractions is shown in Figure 3. Next, CAPRI was used to determine the subsurface stress field, $\sigma_{ij}(x,y)$, under the contact due to $p(x)$ and $q(x)$. Note the peaks located near the edges of contact in Figure 3. These peaks in the pressure, shear, and the underlying subsurface stresses were driven by the geometry near the edges of contact and typically result in crack initiation and growth from the edge of contact.

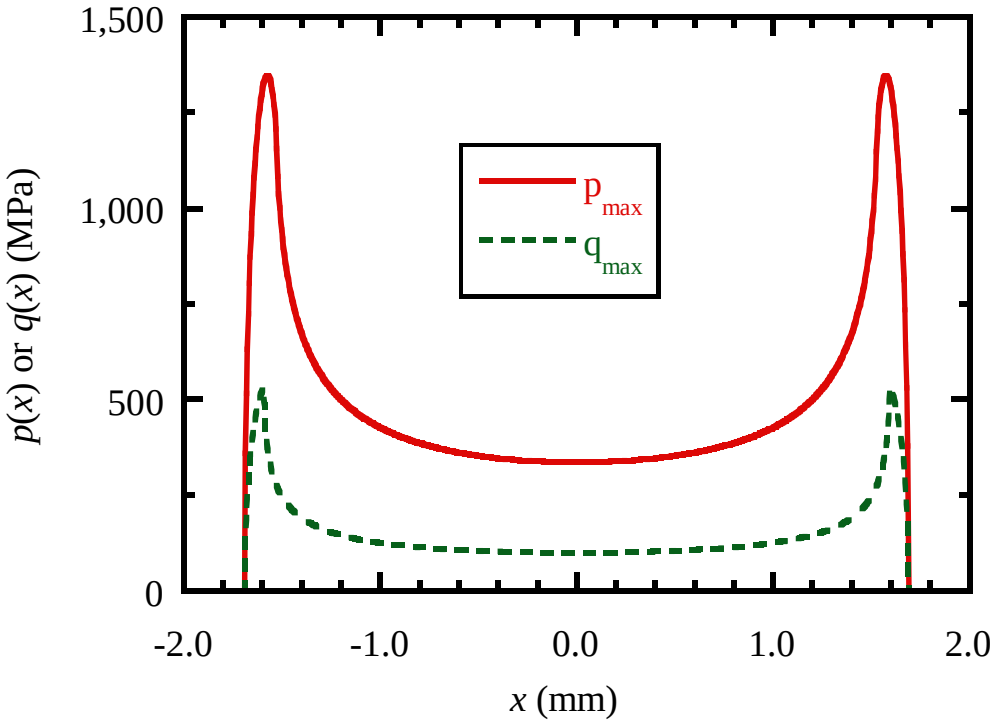

Figure 3: Pressure and shear tractions from CAPRI at maximum applied load

The last step in the analysis was the fracture mechanics based fatigue crack growth prediction. Here, the total stresses along the expected crack growth path were used to calculate the stress intensity factor range, ΔK. To get the total stress solution both the contact stresses from CAPRI and the bulk stress as shown in Figure 1 were superposed. The bulk stress was the

stress distribution induced in the component due to the remotely applied loading and the geometry of the component. A procedure to obtain the bulk stress distribution for a dovetail geometry was described by Golden and Calcaterra [12] which necessitated both the FEM model and CAPRI results. Once the full subsurface stress distribution was known, the mode I stress distribution could be extracted along the expected crack path at the edge of contact. Since this stress distribution was nonlinear, weight function stress intensity factor solutions were applied [16]. The crack propagation life was then integrated using a crack growth model of the form

$$\frac{da}{dN} = f(\Delta K) \tag{2}$$

where d*a*/d*N* is the crack growth rate and the crack growth model *f* is discussed later. Integration of life was performed using the Euler method with small step size starting from a small initial fretting crack typically 25 mm in depth, until fracture. Crack growth properties from previous testing on the same Ti-6Al-4V material used in the US Air Force High Cycle Fatigue program [17] were applied.

3. Statistical Analysis

The random variables for the probabilistic fretting analysis performed in this study were chosen from the key input variables of the deterministic analysis described above. These key input variables included the initial crack size, the coefficient of friction, the slope α that defines the contact forces during partial slip, the crack growth law parameters, and the parameters defining the shape of the pad profile. PDF's were developed for each of these random variables from measurements and test data available both from the dovetail fretting experiments and from other fatigue and fatigue crack growth experiments. The details of the development of these PDF's are described below. A summary of the resulting PDF's are shown in Table 1.

Initial crack size

The deterministic fretting fatigue life prediction analysis described above was a fracture mechanics based crack propagation calculation. To perform this analysis an initial crack size was required. Previous work [16] has shown that the initial fretting cracks tend to be shallow, low aspect ratio (a/c) surface cracks that often appear to be several micro-cracks that have coalesced. Here, a is the surface crack depth and c is the half surface length. Investigations of naturally initiated cracks in smooth bar fatigue specimens in Ti-6Al-4V with the same microstructure [18] have revealed that the cracks appear to initiate almost exclusively at primary alpha grains at the surface of the specimen. These naturally initiated cracks in the primary alpha grains form readily identifiable facets on the specimen fracture surface. Measurements of these initial cracks were made in a prior study [18] on fatigue variability of Ti-6Al-4V, where repeated tests were conducted at a few constant amplitude stress levels. The resulting distribution of primary alpha grain facets was used here to represent the expected variability in initial fretting crack depth. It is therefore assumed in this analysis that the naturally initiated fretting cracks also form at the surface primary alpha grains, albeit at a different local stress state and surface condition as in the prior study. Since it has been shown that typically multiple surface cracks form and coalesce in fretting, a constant, low aspect ratio of $a/c = 0.2$ was used. The mean and standard deviation of the measured naturally initiated crack sizes is listed in Table 1. It was determined that a lognormal distribution was the best fit to the data.

Coefficient of friction and the partial slip slope

As described above and depicted in Figure 2, the coefficient of friction and the partial slip slope of Q versus P were measured during each test. The accuracy of these measurements, however, was limited to the accuracy of the strain gage instrumentation of the tests and the finite

element analysis that was used to convert fixture strain to applied load. Additionally, variability in friction was expected from test to test. Both the measurement uncertainty and inherent variability in the tests needed to be captured in the probabilistic model. To achieve this, data was collected from twenty-three fretting tests all of which were conducted under similar loading conditions. All tests were bare Ti-6Al-4V on Ti-6Al-4V contact (no coatings) and all were loaded at $R = 0.1$. The measured values of friction coefficient and partial slip slope, α, were found to be correlated. The uncertainty in the expected values of friction and partial slip slope along with their correlation was modeled using a multivariate normal distribution. In order to avoid the possibility of an infinite slope, α, the value $1/\alpha$ is used in the analysis procedure and tabulated in Table 1.

Fatigue crack growth parameters

The crack growth rate curves used for crack propagation predictions were based on fatigue crack growth tests previously conducted [17]. Four tests conducted at R = 0.1 and -1 from two different labs were fit to a bilinear crack growth model, where, da/dN is the crack growth rate and ΔK is the stress intensity factor range. These data are plotted in Figure 4. The Walker model [19] was used to collapse the data from the different R values using an equation of the form

$$\begin{aligned} da/dN &= C_1\left[\Delta K(1-R)^{(m-1)}\right]^{n_1} \quad \Delta K < b \\ da/dN &= C_2\left[\Delta K(1-R)^{(m-1)}\right]^{n_2} \quad \Delta K > b \end{aligned} \tag{3}$$

where b is the intersection point for regions 1 and 2, defined as

$$b = \frac{\log_{10} C_1 - \log_{10} C_2}{n_2 - n_1} \tag{4}$$

and the values of the Walker exponent m were determined in the previous program [9]. Different values were used for $R < 0$, $m = 0.275$, and $R > 0$, $m = 0.72$. The statistics of the curve

fit were modeled using a multivariate normal. The coefficients C_i and the exponents n_i were found to be correlated for each segment of the bilinear crack growth model. The mean, standard deviation, and correlation coefficients are summarized in Table 1. The values of the model parameters resulted units of MPa$\sqrt{}$m for ΔK, and m/cycle for da/dN. The da/dN versus ΔK curves for one-hundred randomly generated realizations of C_i and n_i were also plotted in Figure 4.

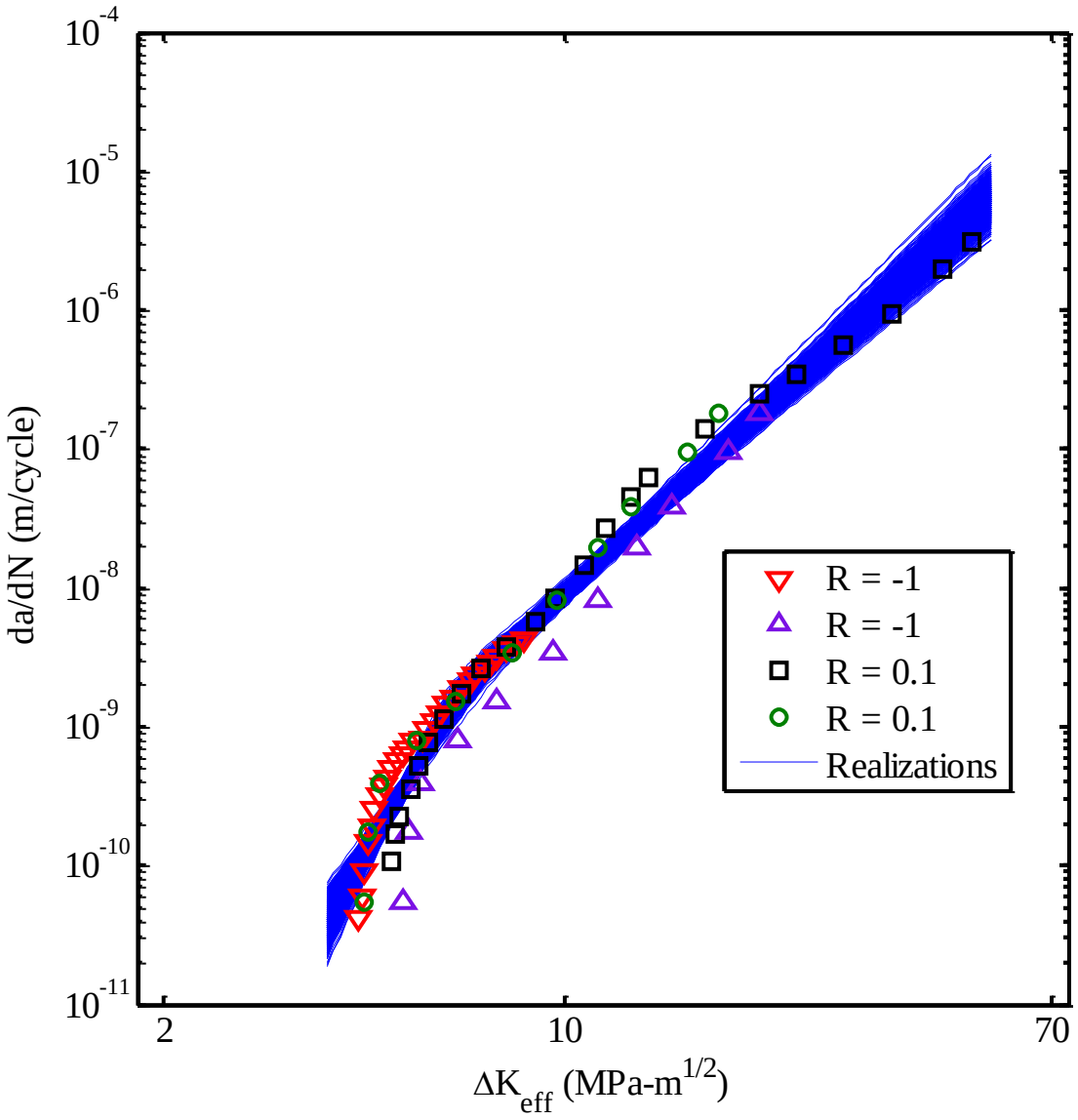

Figure XX: Plot of da/dN versus ΔK data and 100 realizations of the bilinear model.

Pad profile

The nominal geometry for the contact pad is the thick black line shown in Figure 5. The prescribed profile is the geometry that was requested on the part drawings provided to the machine shop. The central segment of the prescribed profile is flat with a length of 3.00 mm. The flat section is flanked by blending radii of 3.0 mm. Due to machining variations, however, the as-machined profiles differ from the prescribed profile in the part drawing and were measured using a contacting profilometer prior to being tested. The contact profilometer had a vertical resolution of approximately 10 nm. Two examples of measured profiles are plotted in Figure 2. Note that the scale on the y-axis is significantly magnified to highlight variations in the measured profiles. It is clear from these measurements that the central flat section of the pad is not truly flat and that the radii at the edges do not always match the prescribed radii either in position or sharpness. Additionally, there is measurable variability in the profile geometry from pad to pad. It was desired to capture this variability through a statistical analysis so it could be used in the subsequent probabilistic analysis. To achieve that objective, seventy-seven contact pads were measured.

In order to model the contact profile variability in the probabilistic analysis, a mathematical description of the contact profile was needed that could capture the important features of the profile. Key features were believed to be the actual radii of the edges of the pad as these can significantly affect the stress at the edge of contact. Also important was the flatness of the central portion of the pad. A rounded pad versus a very flat pad could also significantly affect the contact stresses. A piecewise curve with twenty-one parameters was defined to represent the measured contact profiles and was written as

$$y = \begin{cases} k^L x + b^L & x < a_1 \\ y_0^L + \sqrt{(R^L)^2 - (x - x_0^L)^2} & a_1 < x < a_2 \\ c_0 + c_1 x + c_2 x^2 + c_3 x^3 + c_4 x^4 + c_5 x^5 + c_6 x^6 & a_2 < x < a_3 \\ y_0^R + \sqrt{(R^R)^2 - (x - x_0^R)^2} & a_3 < x < a_4 \\ k^R x + b^R & x > a_4 \end{cases} \quad (5)$$

where x and y represent a Cartesian coordinate system with x along the profile and y is the height of the profile. In the current problem the pad profile is pressed into a flate plate so the function y is also the gap function h. The central segment of the profile ($a_2<x<a_3$) was represented by a sixth order polynomial to allow the nominally flat section to have curvature. Just outside the central section were two circular arcs to represent the radii at the edges of contact. Just beyond the radii were flat taper sections. Through various constraints at $x = a_1 - a_4$, the number of parameters was reduced from twenty-one to thirteen. These thirteen variables k^L, k^R, b^L, b^R, y_0^L, x_0^L, x_0^R, R^L, R^R, c_1, c_2, c_3, c_4, c_5, and c_6 were determined from nonlinear regression of each of the measured seventy-seven profiles. These variables were referred to as γ_i, where i ranged from 0 to 12. The remaining 8 variables in Equation 1 were functions of γ_i as defined by the constraints. The correlation coefficients for γ_i are listed in Table 2, showing high correlation among some of the variables. Finally, the results of the nonlinear regression from all 77 profiles were fit to a multivariate normal distribution. The mean and standard deviation of the regression parameters are listed in Table 1. These variable values will result in a pad profile or gap function, h, with units of μm. Three sample realizations of these fitted profiles are plotted in Figure 6 along with the prescribed profile. The measured and the sampled profiles often differ significantly from the prescribed profile, particularly near the edge of contact.

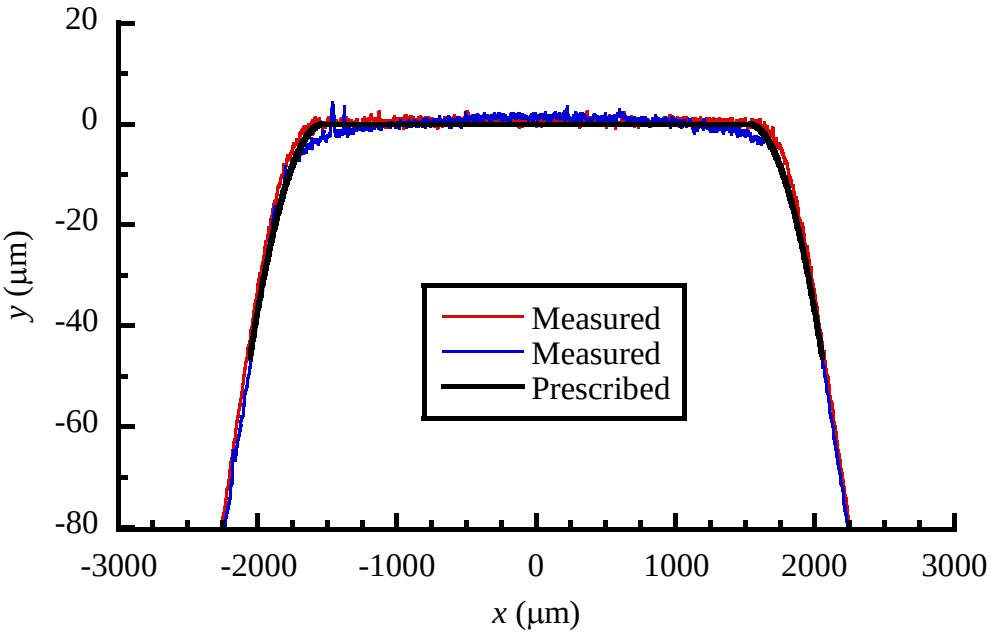

Figure 5: Prescribed and sample measured pad profiles.

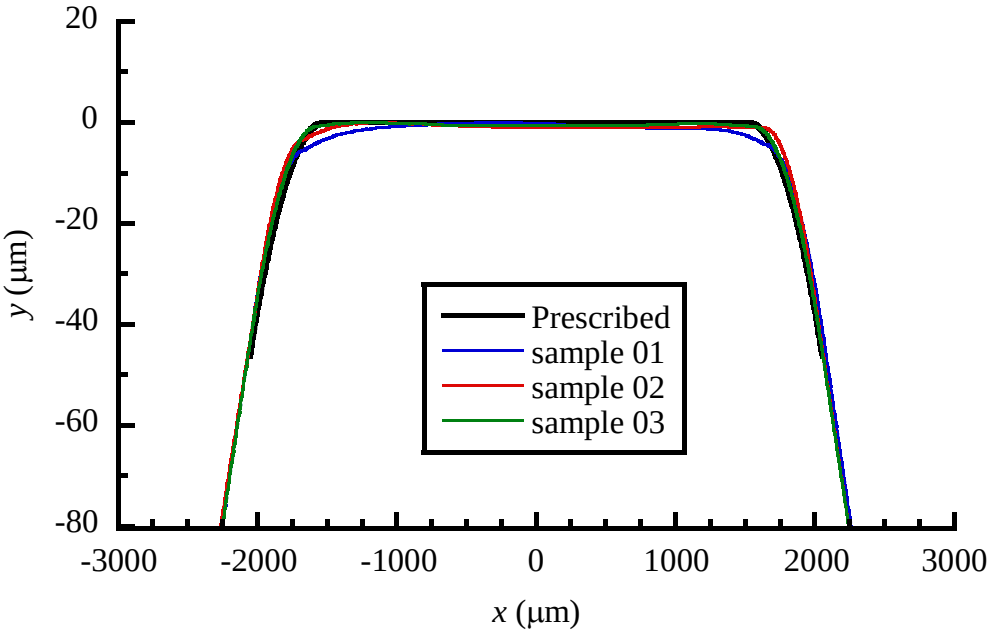

Figure 6: Random realizations of the pad profile model compared to the prescribed profile.

Table 1: Summary of random variable statistics.

Random Variable	No.	Mean	St. Dev.	Distribution Type
Initial crack size, a_i (μm)	X_1	15.1	8.48	Lognormal
Friction coefficient, μ_{ave}	X_2	0.302	0.021	Correlated normal
Partial slip slope, α	X_3	1.96	0.120	ρ_{23} = - 0.375
Crack growth, $\log_{10}(C_1)$	X_4	-14.6	0.486	Correlated normal
Crack growth, n_1	X_5	7.19	0.715	ρ_{45} = -0.9973
Crack growth, $\log_{10}(C_2)$	X_6	-11.8	0.157	Correlated normal
Crack growth, n_2	X_7	3.81	0.146	ρ_{67} = -0.9751
Profile, $\gamma_0 = k^L$	X_8	0.181	$5.84\text{x}10^{-3}$	Correlated normal
Profile, $\gamma_1 = y_0^L$	X_9	-2335	410	(see Table XX)
Profile, $\gamma_2 = R^L$	X_{10}	2333	411	
Profile, $\gamma_3 = x_0^L$	X_{11}	-1612	37.7	
Profile, $\gamma_4 = R^R$	X_{12}	2289	379	
Profile, $\gamma_5 = x_0^R$	X_{13}	1620	35.4	
Profile, $\gamma_6 = k^R$	X_{14}	-0.183	$4.96\text{x}10^{-3}$	
Profile, $\gamma_7 = c_1$	X_{15}	$-2.00\text{x}10^{-4}$	$6.20\text{x}10^{-4}$	
Profile, $\gamma_8 = c_2$	X_{16}	$-1.21\text{x}10^{-6}$	$1.01\text{x}10^{-6}$	
Profile, $\gamma_9 = c_3$	X_{17}	$1.53\text{x}10^{-10}$	$6.38\text{x}10^{-10}$	
Profile, $\gamma_{10} = c_4$	X_{18}	$9.80\text{x}10^{-13}$	$6.16\text{x}10^{-13}$	
Profile, $\gamma_{11} = c_5$	X_{19}	$-3.77\text{x}10^{-17}$	$1.87\text{x}10^{-16}$	
Profile, $\gamma_{12} = c_6$	X_{20}	$-3.80\text{x}10^{-19}$	$1.59\text{x}10^{-19}$	

Table 2: Pad profile regression correlation coefficients

	γ_0	γ_1	γ_2	γ_3	γ_4	γ_5	γ_6	γ_7	γ_8	γ_9	γ_{10}	γ_{11}	γ_{12}
γ_0	1	-0.079	0.078	-0.119	-0.051	0.184	-0.364	0.153	0.175	-0.107	-0.130	0.073	0.112
γ_1	-0.079	1	-1.000	-0.921	-0.404	0.321	-0.122	0.093	-0.205	-0.203	0.281	0.275	-0.246
γ_2	0.078	-1.000	1	0.921	0.404	-0.321	0.121	-0.092	0.207	0.203	-0.282	-0.275	0.247
γ_3	-0.119	-0.921	0.921	1	0.325	-0.372	0.270	-0.019	0.104	0.136	-0.201	-0.247	0.219
γ_4	-0.051	-0.404	0.404	0.325	1	-0.899	-0.204	-0.102	0.079	0.065	-0.116	0.002	0.123
γ_5	0.184	0.321	-0.321	-0.372	-0.899	1	-0.033	0.010	-0.004	0.062	0.021	-0.147	-0.061
γ_6	-0.364	-0.122	0.121	0.270	-0.204	-0.033	1	-0.095	-0.242	-0.017	0.142	0.078	-0.133
γ_7	0.153	0.093	-0.092	-0.019	-0.102	0.010	-0.095	1	0.140	-0.876	-0.027	0.627	0.059
γ_8	0.175	-0.205	0.207	0.104	0.079	-0.004	-0.242	0.140	1	-0.099	-0.869	0.057	0.765
γ_9	-0.107	-0.203	0.203	0.136	0.065	0.062	-0.017	-0.876	-0.099	1	0.011	-0.915	-0.027
γ_{10}	-0.130	0.281	-0.282	-0.201	-0.116	0.021	0.142	-0.027	-0.869	0.011	1	0.027	-0.944
γ_{11}	0.073	0.275	-0.275	-0.247	0.002	-0.147	0.078	0.627	0.057	-0.915	0.027	1	-0.031
γ_{12}	0.112	-0.246	0.247	0.219	0.123	-0.061	-0.133	0.059	0.765	-0.027	-0.944	-0.031	1

4. Probabilistic Analysis

Monte Carlo sampling was carried out to determine the moments (mean and standard deviation) of the cycles-to-failure distribution. This procedure involved repeated generation of realizations of the random variables and execution of the deterministic fretting fatigue algorithm to determine cycles-to-failure. The deterministic fretting fatigue algorithm was simplified as much as possible to minimize the computational time needed for each set of random variable samples. All necessary calculations were performed using MATLAB since both CAPRI and the crack growth calculation code were developed using MATLAB. This included calculation of the contact forces using the method demonstrated by Gean and Farris [6], rather than modeling the contact in a FEM analysis. The CAPRI run time was minimized by reducing the number of Fast Fourier Transform terms to the minimum required and optimizing the solver parameters for this problem. Finally, a linear fit of the bulk stresses as a function of the contact forces was created from a series of FEM analyses, rather than using a new FEM analysis for each Monte Carlo run. Eliminating the FEM analyses from the calculation of fretting fatigue life reduced the computational time to approximately 1.2 s per simulation when running in parallel with 4 processors on an Intel Xeon quad core workstation. This made running the Monte Carlo analysis with a significant number of samples possible. The ensemble of cycles to failure, N_f, results were then analyzed to determine the mean and standard deviation. Sufficient samples were executed to ensure high confidence in the computed moments.

Probabilistic sensitivities play an important role in determining insight into the dominant factors governing a probabilistic analysis and provide information as to potentially effective methods to improve the reliability. There are a number of methods in the literature such as

scatter plots [20], Pearson or Spearman correlation [21], regression methods [22], and the Score function method [23], among others, that can provide useful information. The following is a description of several methods used in the current work.

Scatter plots

Scatter plots are a two-dimensional point plot of the sample points versus the corresponding response points. The sample realizations for each random variable (X) and the corresponding results (Y) are plotted on separate axes. If a random variable is not important, no pattern should be discernable, that is, the samples for X should mimic its marginal distribution. Conversely, if a random variable is important, the pattern of realizations for X will be distinctly non-random. Scatterplots are an inexpensive but qualitative method.

Regression and correlation

Linear regression (LR) methods are well known and widely available tools for assessing variance contribution. LR approximates the relationship between response and the random variables as

$$y(\boldsymbol{X}) = \beta_0 + \sum \beta_i f(X_i) \tag{6}$$

where f is an arbitrary function of the random variable X_i. In general, LR may contain quadratic and interaction terms of any number of the variables, X_i.

The results from an LR model provide an easy mechanism to estimate the sensitivities of the response (denoted Z) standard deviation (σ_Z) to the standard deviation of the input parameters (σ_i), e.g., $\partial\sigma_Z/\partial\sigma_i$, or of the response mean (μ_Z) to the mean of the input parameters (μ_i), e.g., $\partial\mu_Z/\partial\mu_i$. This sensitivity in its nondimensionalized form $\partial\sigma_Z/\partial\sigma_i * \sigma_i/\sigma_Z$ or $\partial\mu_Z/\partial\mu_i * \mu_i/\mu_Z$ provides an indication as to the relative importance of the random variables and can be used to estimate design improvements.

One of the simplest linear regression models in terms of the original variables is

$$Z = A_0 + A_1 X_1 + \cdots + A_n X_n \tag{7}$$

In order to simplify the sensitivity equations derived below, Equation 1 can be rewritten as the standardized model

$$\frac{Z - \bar{Z}}{S_Z} = \hat{A}_1 \frac{(X_1 - \mu_1)}{\sigma_1} + \cdots + \hat{A}_n \frac{(X_n - \mu_n)}{\sigma_n} \tag{8}$$

where $\bar{Z}$ denotes the sampling mean of the response and S_Z represents the sampling standard deviation of Z. Equation 2 can then be rewritten

$$\hat{Z} = \hat{A}_1 \hat{X}_1 + \cdots + \hat{A}_n \hat{X}_n \tag{9}$$

where the conversion between the original and standardized coefficients is

$$A_i = \frac{\sigma_Z}{\sigma_i} \hat{A}_i \tag{10}$$

$$A_0 = \bar{Z} - A_1 \mu_1 - \cdots - A_n \mu_n \tag{11}$$

It is known that for a linear model of the form $Z = A_0 + A_1 X_1 + \cdots + A_n X_n$ that the expected value or mean value of Z can be written

$$E(Z) = \sum_{i=1}^{n} A_i E(X_i) \tag{12}$$

and the sensitivities or partial derivatives are simply

$$\frac{\partial \mu_Z}{\partial \mu_i} = A_i \tag{13}$$

The variance of Z can be written as

$$Var(Z) = \sum_{i=1}^{n} \sum_{j=1}^{n} A_i A_j \rho_{ij} \sigma_i \sigma_j \tag{14}$$

[24] and the sensitivities or partial derivatives are [25]

$$\frac{\partial \sigma_Z}{\partial \sigma_i} = \frac{A_i}{\sigma_Z} \sum_{j=1}^{n} A_j \rho_{ij} \sigma_j \tag{15}$$

For independent variables ($\rho_{ij} = 0$) this reduces to

$$\frac{\partial \sigma_Z}{\partial \sigma_i} = \frac{\sigma_i}{\sigma_Z} A_i^2 \tag{16}$$

Note, based on Eq. (10), the sensitivity must be positive, whereas, based upon Eq. (9), the sensitivity can be negative for negative correlation coefficients.

Rewriting the sensitivity in terms of standardized regression coefficients yields

$$\frac{\partial \sigma_Z}{\partial \sigma_i} = \frac{\sigma_Z}{\sigma_i} \frac{\hat{A}_i}{\sigma_Z} \sum_{j=1}^{n} \frac{\sigma_Z}{\sigma_j} \hat{A}_j \rho_{ij} \sigma_j = \frac{\sigma_Z}{\sigma_i} \hat{A}_i \sum_{j=1}^{n} \hat{A}_j \rho_{ij} \tag{17}$$

Nondimensionalizing yields

$$S_i = \frac{\partial \sigma_Z}{\partial \sigma_i} \frac{\sigma_i}{\sigma_Z} = \frac{\sigma_i}{\sigma_Z} \frac{\sigma_Z}{\sigma_i} \hat{A}_i \sum_{j=1}^{n} \hat{A}_j \rho_{ij} = \hat{A}_i \sum_{j=1}^{n} \hat{A}_j \rho_{ij} \tag{18}$$

For independent variables this reduces to

$$S_i = \frac{\partial \sigma_Z}{\partial \sigma_i} \frac{\sigma_i}{\sigma_Z} = \hat{A}_i^2 \tag{19}$$

Finite Difference

The finite difference (FD) method [26] was used in this study to compute the probabilistic sensitivities as a method of verifying other much more efficient methods such as LR. FD is conducted by simply applying a small change in a random variable parameter (mean or standard deviation) and then re-running the Monte-Carlo analysis to obtain a new response distribution. The change in the modes of the response distribution divided by the change in the random variable parameter, i.e. $\Delta\sigma_Z/\Delta\sigma_i$, gives an estimate of the probabilistic sensitivity, $\partial\sigma_Z/\partial\sigma_i$. Calculation of the probabilistic sensitivities using FD can be very computationally costly due to the large number of Monte Carlo simulations required. In the current problem there

are 20 random variables each with 2 parameters (mean and standard deviation) multiplied by a sample size of 50,000 for each parameter results in 2 million simulations or approximately 1 month computation time. 50,000 was chosen as a necessary balance between accuracy and computational cost. Unfortunately it is unlikely to be enough samples to achieve convergence in the sensitivity estimate. In fact, additional simulations were performed to double the sample size to 100,000 for the FD analysis of several variables of interest proving the estimates were either converged (less than 5% change) or in some cases not converged. However, of those variables of interest that were not converged changes in the estimates with sample size of 100,000 were modest, i.e. 30% or less. A percent change in sensitivity estimates for many variable parameters were not considered since the estimates were nearly zero.

5. Results and Discussion

Probabilistic Life Prediction

The probabilistic fretting fatigue life prediction tool was exercised at several experimental load cases. Results were generated at the 5 applied loading conditions (F_{max} = 18, 20, 22, 24, and 30 kN) used in the dovetail testing program. Lives were generated at each loading condition initially using a sample size of 10,000 for the random variables initial crack size, coefficient of friction, partial slip slope, crack growth curve, and the pad profile. These results are plotted on lognormal probability paper in Figure 7 along with the experimental lives. The solid lines are the distribution of the Monte Carlo predicted failure lives with the applied highest load (30 kN) on the left and the lowest applied load (18 kN) on the right. The experimental lives shown were as follows: 1,371,000, 10,000,000, and 693,000 cycles at 18 kN; 995,000 and 919,900 cycles at 20 kN; 249,900, 346,200, and 497,800 cycles at 22 kN; 164,000 cycles at 24 kN; and 105,000 cycles at 30 kN. These data were quite limited for an evaluation of

a probabilistic life prediction, however, they were still useful to ensure the predictions were near the test results. The comparison in Figure 7 shows that at the higher loads the predictions were closer than at the lower loads. Not surprisingly, all of the experimental results fall within the scatter of the simulated results. At the lower applied loads, however, the test results seem to deviate from the predictions by having longer lives. In fact, the longest life at 18 kN is over 10 million cycles (test was a run-out) which was at the 99% probability level of the prediction. If the three 18 kN experiments do belong to the simulated failure life distribution there is less than a 3% chance that this long life would occur in testing. This shows that the fracture mechanics life prediction model is likely missing some of the physics of the problem. It supports the view that crack nucleation or formation may be a significant portion of the life at lower stress levels, even for a crack propagation model has an initial crack size at a microstructural scale.

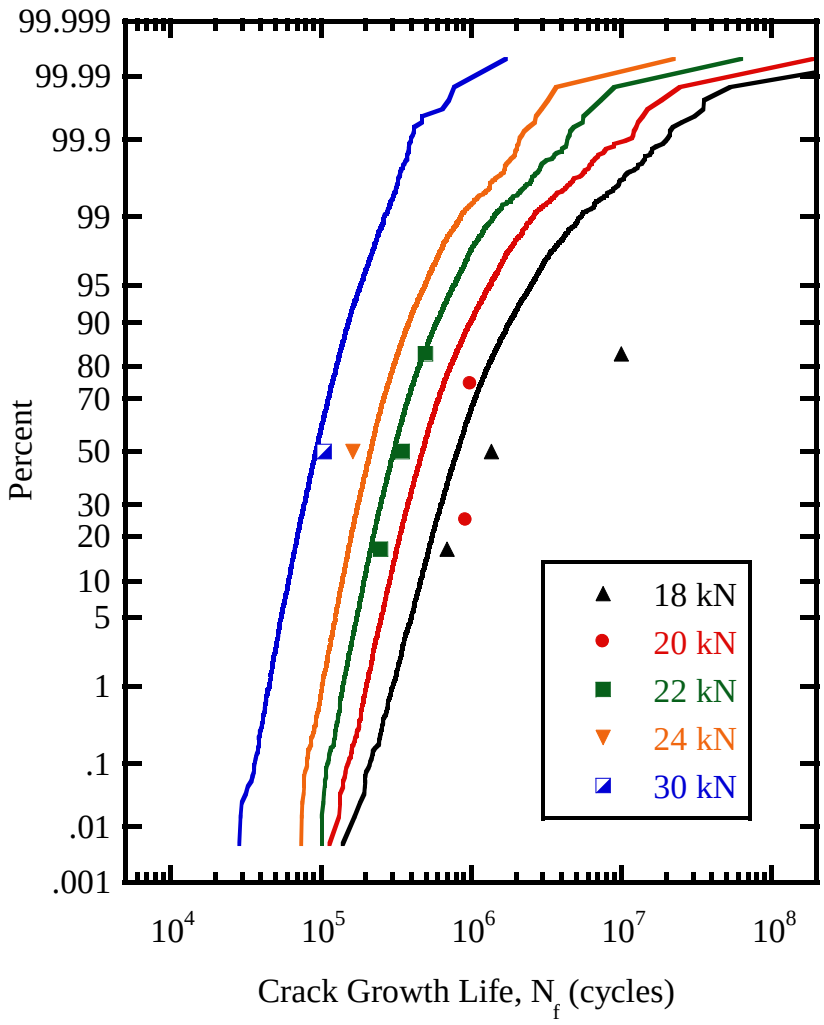

Figure 7: Probability plot of experimental (points) and predicted (lines) lives at several applied loads.

The results plotted in Figure 7 were generated with just 10,000 samples to minimize processing time for each condition analyzed. Since the number of samples was relatively small, an understanding of the variance in the estimates of mean and standard deviation of N_f was important. Variance estimates of the mean and standard deviation of the distribution were calculated at each of the applied forces and listed in Table 3. Since the distribution of N_f was fairly lognormal, the modes of the distribution of the logarithm of N_f were calculated. The estimates for mean of the $\log_{10}$ of N_f were then converted back to cycles. The columns showing

the 95% confidence bounds of the mean were then converted back to cycles or the ratio of the lower bound (LB) and upper bound (UB) to the mean cycle count. The coefficient of variance (COV) was also calculated entirely in log units. Interestingly, the COV decreased with increased applied loading, which was consistent with fatigue test results in Ti-6Al-4V [18] and it is generally true in metallic aerospace materials that at higher stresses the variance in fatigue life decreases. Also, in Table 3 the estimates of the mean and standard deviation of the distribution were calculated for smaller and larger numbers of samples at F_{max} = 22 kN. With more samples, the confidence bounds shrink significantly as expected. In addition to quantifying the modes of the distribution, PDF's were fit to the distribution. Figure 8 is a plot of two PDF types fit to the N_f results at F_{max} = 22 kN. The solid line is a nonparametric kernel estimate of the PDF [26], while the dashed curve was a lognormal fit to the N_f distribution. The differences in the PDF's showed that the distribution of failure lives was skewed toward longer lives and also had a higher peak. This skewness toward longer lives in the tail can also be observed in Figure 7, and this trend increased with smaller applied loads.

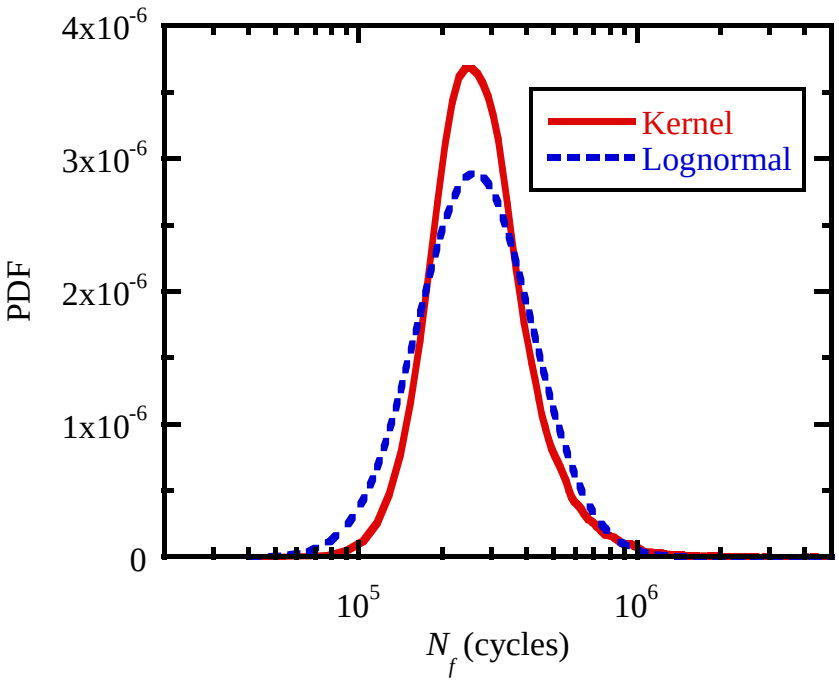

Figure 8: PDF estimates of N_f for 10,000 simulations at F_{max} = 22 kN.

Table 3: Mean and coefficient of variation (c.o.v.) of the Monte Carlo analysis results including the 95% upper bound (UB) and lower bound (LB) confidence limits

		Mean of $\log_{10}(N_f)$			COV of $\log_{10}(N_f)$		
F_{max} (kN)	Sample Size	LB / Mean	Mean (cycles)	UB / Mean	LB / COV	COV	UB / COV
18 kN	10,000	0.989	872,600	1.012	0.986	4.26%	1.012
20 kN	10,000	0.990	509,900	1.010	0.988	4.01%	1.012
22 kN	1000	0.973	328,400	1.028	0.960	3.54%	1.042
22 kN	10,000	0.991	326,200	1.009	0.987	3.72%	1.013
22 kN	500,000	0.999	324,300	1.001	0.998	3.70%	1.002
24 kN	10,000	0.992	225,400	1.008	0.989	3.51%	1.014
30 kN	10,000	0.993	95,400	1.007	0.988	3.24%	1.012

Sensitivity Results

Perhaps the simplest method to qualitatively determine sensitivity is through a scatter plot. Figure 9 below shows the scatter plots that relate cycles-to-failure (y axis) with each random variable (x axis) for 10,000 samples. The scatter plot for random variable X_2 shows a definite pattern. Correlation coefficients (Pearson or Spearman) for each variable relate to the amount of variance in Y that can be apportioned to X_i. The results for Pearson correlation

coefficients, given in Table 4, indicate that variable X_2 (coefficient of friction) is by far the dominant variable, contributing 65% of the variance in N_f. It must be pointed out, however, that the correlation coefficients are obtained without consideration for the simultaneous variations in other random variables. A better estimate of variable importance can be determined using linear regression, discussed below.

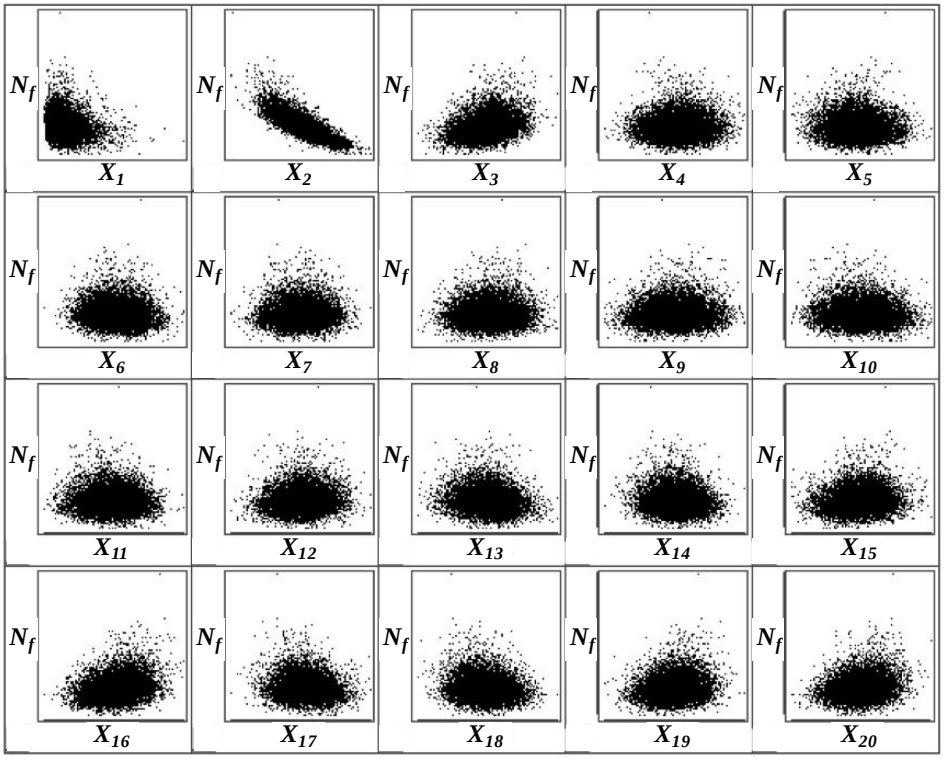

Figure 9: Scatter plots of the model output cycles to failure, N_f, versus the input random variables, X_1 through X_{20}

In this research, an LR model of the form of Equation 6 was used, where $\boldsymbol{X}$ denotes a vector of random variables, y represents the cycles-to-failure and the β's are coefficients that are fit to the analytical results. Table 5 shows the results of a "best model" fit using a specified number of variables. For example, using only 2 variables, the combination of X_2 and X_{16} account for the largest percentage of the variance in N_f. Note, once X_2 is included in the model, adding X_{16} adds 17 percent to the R^2 sum, however, the R^2 value using the Pearson correlation

coefficient for X_2 without considering any other random variables is 25%. From the results, one can see quickly the diminished returns offered after the first few random variables. For example, if only 5 random variables are used in an LR model, this model would account for 85% out of a possible 91% of the output variance. It is somewhat surprising that a simple linear model with respect to the random variables can account for such a large percentage of the output variance.

Table 4: R^2 values for the random variables

Variable	R^2
X_1	0.024
X_2	0.645
X_3	0.093
X_4	0.001
X_5	0.002
X_6	0.006
X_7	0.002
X_8	0.002
X_9	0.004
X_{10}	0.004
X_{11}	0.003
X_{12}	0.005
X_{13}	0.017
X_{14}	0.008
X_{15}	0.007
X_{16}	0.063
X_{17}	0.013
X_{18}	0.020
X_{19}	0.020
X_{20}	0.038

Table 5: Best model linear regression results

N	R^2	$C(p)$	Random Variables in Model									
1	0.645	28,370	X_2									
2	0.713	21,020	X_2	X_{16}								
3	0.754	16,620	X_2	X_9	X_{10}							
4	0.824	9000	X_2	X_{16}	X_{18}	X_{20}						
5	0.846	6660	X_1	X_2	X_{16}	X_{18}	X_{20}					
6	0.855	5710	X_1	X_2	X_{13}	X_{16}	X_{18}	X_{20}				
7	0.874	3640	X_1	X_2	X_6	X_7	X_{16}	X_{18}	X_{20}			
8	0.883	2690	X_1	X_2	X_6	X_7	X_{13}	X_{16}	X_{18}	X_{20}		
9	0.898	1060	X_1	X_2	X_6	X_7	X_{16}	X_{17}	X_{18}	X_{19}	X_{20}	
10	0.901	720	X_1	X_2	X_6	X_7	X_{13}	X_{16}	X_{17}	X_{18}	X_{19}	X_{20}

Table 6 shows the results using LR considering natural groupings of random variables. The variables were partitioned into 4 groups: (X_1 - initial crack size, X_2-X_3 coefficient of friction – partial slip slope, X_4-X_7 crack growth parameters, X_8-X_{20} geometry profile). The results indicate that group 2 is dominant, followed by the geometry profile. Surprisingly, the traditionally dominant random variables in fatigue, crack growth rate and initial crack size are not significant in terms of their contribution to the output variance, e. g., these parameters could be modeled deterministically.

Table 6: Linear regression group analysis showing the effect of each random variable group on the model R^2

Group	RV Added	# RV	Model R^2	R^2	$C(p)$	F value
1	X_2, X_3	2	0.645	0.645	28,370	9080
2	$X_8 - X_{20}$	15	0.210	0.855	5710	1110
3	$X_4 - X_7$	19	0.030	0.885	2420	660
4	X_1	20	0.022	0.908	20	2410

Next, we wish to quantify the probabilistic sensitivities, particularly the sensitivity of the standard deviation of the response (life) to the random variable parameters mean, $\partial\sigma_Z/\partial\mu_i$, and standard deviation, $\partial\sigma_Z/\partial\sigma_i$. Figure 10 is a bar chart of the normalized sensitivity of the standard deviation of the cycles to failure, N_f, response, denoted Z, to the standard deviation of the random variables, X_i, simply denoted by i in Equation 19. Results from the finite difference

analysis and linear regression show very good agreement. The analysis shows that the standard deviation of the response is by far most sensitive to the standard deviation of the coefficient of friction (X_2) and to several parameters of the flat section of the contact profile (X_{16} - X_{20}). The slope of the first segment of the bilinear crack growth law (X_5) and the intercept of the second segment (X_6) also have relatively high sensitivities. Also notable is the sensitivity of the initial crack size (X_1) is quite small. The sensitivities of these variables is essential to understand when evaluating which variables are most important to the process being analyzed. One must also consider, however, the likelihood that the estimates of these random variable parameters will change due to additional or better quality data, or that these parameters can change through an alteration to the system, i.e. machining tolerances or addition of coatings.

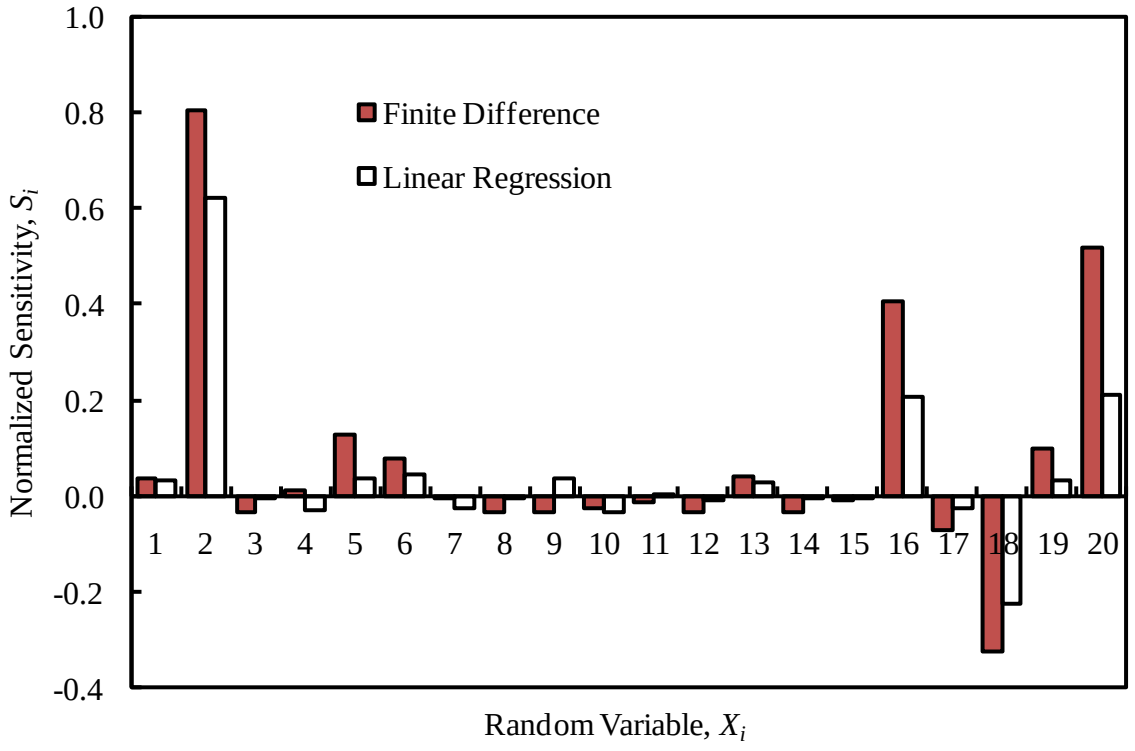

Figure 10: Comparison of S_i for FD and LR.

Figure 10 helped to identify that the standard deviation of X_{16}, X_{18}, and X_{20} were parameters with a relatively high sensitivity. It is not intuitive, however, how these variables

affect the pad profile. Further analysis of the profile has shown that the flatness of the "flat" section ($a_2 < x < a_3$) of the pad profile is strongly affected by the values of these variables. Here, flatness is defined as the peak to peak height difference in y. A probabilistic fretting analysis was performed the pad profile being the only group of random variables. The remaining variables were deterministic. The results showed a significant correlation between $\log_{10} N_f$ and X_{16}, X_{18}, and X_{20} of 0.35 to 0.55, however, the correlation between $\log_{10} N_f$ and flatness was 0.77. Figure 11 is a scatter plot showing this relationship.

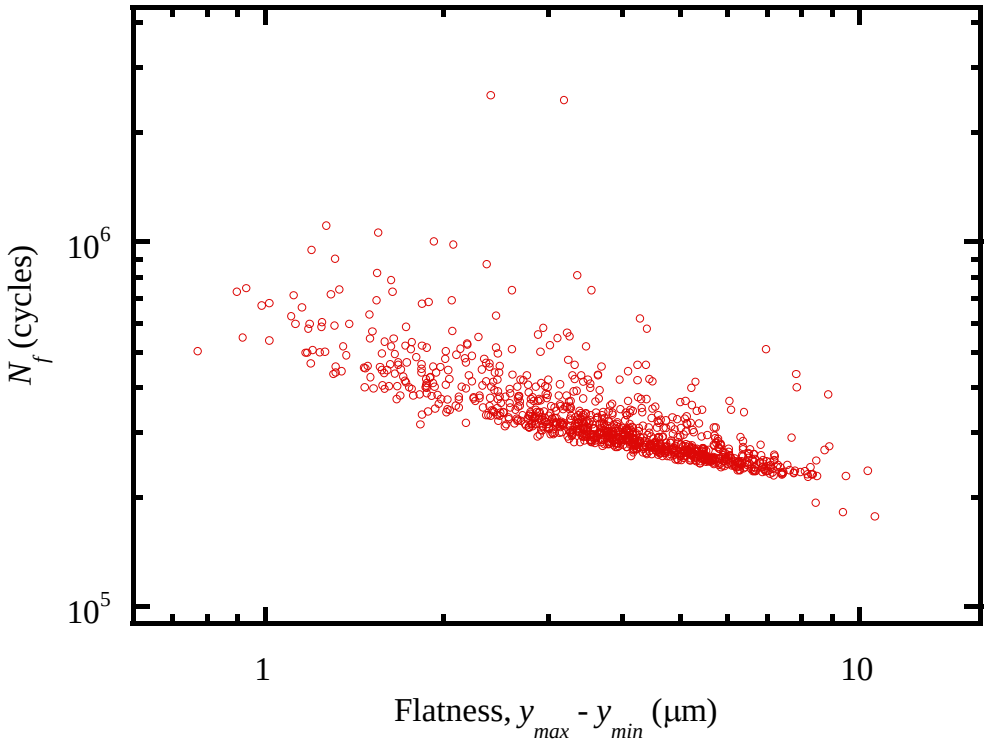

Figure 11: Scatter plot of fatigue crack growth life versus profile flatness showing far stronger correlation than with any of the random variables.

6. Conclusions

A new probabilistic fretting analysis was developed to investigate the relative importance of typical fretting input variables on the predicted failure lives. Several random variable inputs were identified and PDF's were quantified using laboratory data. Monte Carlo sampling of the

input PDF's was performed and a deterministic analysis was repeatedly run using the sampled inputs to obtain a distribution of predicted fretting lives. The results were compared to experimental fretting fatigue tests and the predictions were much closer at higher stresses than at lower stress possibly due to substantial crack nucleation lives at the lower stresses. The results showed that considerable scatter in fretting lives can be expected based on variability in the material properties, contact profiles, coefficient of friction, and contact force response. Interestingly, the dominant variables in terms of contribution to the cycles-to-failure variance were the coefficient of friction and several terms within the geometry profile; whereas, the traditionally dominant variables in fatigue crack growth analyses, initial crack size and crack growth, were not as significant.

Acknowledgements

The authors would like to thank Prof. Farris and his students at Purdue University for providing the CAPRI software used in this study. This work was partially supported by the Air Force Research Laboratory, Materials and Manufacturing Directorate through subcontract USAF-5212-STI-SC-0021 from General Dynamics Information Technology to the University of Texas at San Antonio.

References

[1] Dang Van K, "Macro–micro approach in high-cycle multiaxial fatigue," In: D.L. McDowell and R. Ellis, Editors, Advances in Multiaxial Fatigue, ASTM STP 1191, Philadelphia (1993), pp. 120–130.

[2] Lykins CD. Mall S. Jain V. An Evaluation of Parameters for Predicting Fretting Fatigue Crack Initiation. Int J Fatigue. 2000;22:703-716.

[3] Fridrici V, Fouvry S, Kapsa P, Perruchaut P, "Prediction of Cracking in Ti–6Al–4V Alloy Under Fretting-Wear: Use of the SWT Criterion," Wear 2005, 259, pp 300-308.

[4] Murthy, "Fretting Fatigue of Ti-6Al-4V Subjected to Blade/Disk Contact Loading," Developments in Fracture Mechanics for the New Century, 50th Anniversary of Japan Society of Materials Science, Osaka, Japan, pp. 41-48, 2001.

[5] Rooke DP, Jones, DA. Stress Intensity Factors in Fretting Fatigue. J Strain Analysis 1979;14:1-6.

[6] Hattori T, Nakamura M, Sakata H, Watanabe T. Fretting Fatigue Analysis Using Fracture Mechanics. JSME Int J 1988;31:100-107.

[7] Chan KS, Yi-Der Lee, Davidson DD, Hudak SJ, Jr. A Fracture Mechanics Approach to High Cycle Fretting Fatigue Based on the Worst Case Fret Concept. Int J Fracture 2001;112:299-330.

[8] Kumari S, Farris, TN, "Statistical Analysis of Effect of Contact Surface Profile on Fretting Fatigue Life for Ti-6Al-4V," 47th AIAA/ASME/ASCE/AHS/ASC Structures, Structural Dynamics, and Materials Conference, AIAA 2006.

[9] Zhang R, Mahadevan S, "Probabilistic Prediction of Fretting Fatigue Crack Nucleation Life of Riveted Lap Joints," 41st AIAA/ASME/ASCE/AHS/ASC Structures, Structural Dynamics, and Materials Conference, AIAA-2000-1645, 2000.

[10] Chevalier L, Cloupet S, Soize C, "Probabilistic Model for Random Uncertainties in Steady State Rolling Contact," Wear 2005, 258, pp 1543-1554.

[11] Golden PJ, Nicholas T, "The Effect of Angle on Dovetail Fretting Experiments in Ti-6Al-4V," Fatigue and Fracture of Engineering Materials and Structures, 28, 2005, pp. 1169-1175.

[12] Golden PJ, Calcaterra. A Fracture Mechanics Life Prediction Methodology Applied to Dovetail Fretting. Tribology International, Vol. 39, 2006, pp.1172-80.

[13] Gean, M.C., Farris, T.N., "Mechanics Modeling of Firtree Dovetail Contacts," 49th AIAA/ASME/ASCE/AHS/ASC Structures, Structural Dynamics, and Materials Conference, AIAA 2008-2176, 2008.

[14] Chan KS, Enright MP, Moody JP, Golden PJ, Chandra R, Pentz AC, "Residual Stress Profiles for Mitigating Fretting Fatigue in Gas Turbine Engine Disks," Int J Fatigue, Vol. X, 2009, pp. XX-XX.

[15] McVeigh PA, Harish G, Farris TN, Szolwinski MP. Modeling interfacial conditions in nominally flat contacts for application to fretting fatigue of turbine engine components. International Journal of Fatigue , Vol. 21, 1999; pp. S157–65.

[16] Golden, P.J., Grandt, A.F., Jr., "Fracture mechanics based fretting fatigue life predictions in Ti–6Al–4V," Engineering Fracture Mechanics, Vol. 71, 2004, pp. 2229-2243.

[17] Gallagher JP, et al. AFRL-ML-TR-2001-4159, Improved High-Cycle Fatigue (HCF) Life Prediction, Wright-Patterson Air Force Base, OH, 2001.

[18] Golden, P.J., John, R., Porter, W.J., III, "Variability in Room Temperature Fatigue Life of Alpha+Beta Processed Ti-6Al-4V," International Journal of Fatigue, 2009, doi:10.1016/j.ijfatigue.2009.01.005.

[19] Walker, K., "The Effect of Stress Ratio During Crack Propagation and Fatigue for 2024-T3 and 7075-T6 Aluminium," Effects of Environment and Complex Load History on Fatigue Life (10th edn), ASTM STP 462, American Society for Testing of Materials, PA, 1970, pp. 1–14.

[20] J.P.C.Kleijnen, and J.C. Helton, "Statistical Analyses of Scatterplots to Identify Important Factors in Large-scale Simulation, Review and comparison of techniques," Reliability Engineering and System Safety, 65,1999, pp.147-185

[21] D.M. Hamby, "A Review of Techniques for Parameter Sensitivity Analysis of Environmental Models," Environmental Monitoring and Assessment 1994, 32, pp 135-154

[22] N.R. Draper and H. Smith, Applied Regression Analysis, 3rd Ed., Wiley-Interscience, 1998

[23] Rubinstein R.Y. and Shapiro, A. Discrete Event Systems, Sensitivity Analysis And Stochastic Optimization By The Score Function Method. J. Wiley & Sons, Chichester, England, 1993.

[24] Ang H-S.A, Tang WH, *Probability Concepts in Engineering*, Wiley, USA, 2007.

[25] H.R. Millwater, "Universal Properties of Kernel Functions for Probabilistic Sensitivity Analysis," *Probabilistic Engineering Mechanics*, Vol 24, 2009, 89–99

[26] B.W. Silverman, *Density Estimation for Statistics and Data Analysis*, Chapman & Hall/CRC, Baco Raton, FL, 1998